Robotica (2019) volume 37, pp. 1267–1288. © Cambridge University Press 2018
doi:10.1017/S0263574718000929

Optimal design and evaluation of a dexterous 4 DoFs haptic device based on delta architecture

Célestin Préault†, Houssem Saafi‡*, Med Amine Laribi† and Said Zeghloul†

†*Department of GMSC, Pprime Institute, CNRS - University of Poitiers - ENSMA - UPR 3346, Poitiers, France*
‡*Mechanical Laboratory of Sousse, National Engineering School of Sousse, University of Sousse, Sousse, Tunisia*

(Accepted August 15, 2018)

SUMMARY
This paper introduces a novel kinematic of a four degrees of freedom (DoFs) device based on Delta architecture. This new device is expected to be used as a haptic device for tele-operation applications. The challenging task was to obtain orientation DoFs from the Delta structure. A fourth leg is added to the Delta structure to convert translations into rotations and to provide translation of the handle. The fourth leg is linked to the base and to the moving platform by two universal joints. The architecture as well as the kinematic model of the new structure, called 4haptic, are presented. Comparisons in terms of kinematic behavior between the 4haptic device and the existing device developed based on spherical parallel manipulator architecture are presented. The results prove the improved behavior of the 4haptic device offering a singularity-free useful workspace, which makes it a suitable candidate to tele-operated system for Minimally Invasive Surgery. The dimensions of the 4haptic device, having the smallest workspace containing a prespecified region in space, are identified based on an optimal dimensional synthesis method.

KEYWORDS: Delta robot, Haptic devices, Minimally invasive surgery, Tele-operation system, Synthesis, Genetic algorithm

1. Introduction

Haptic devices are developed to simulate interaction between the user and a virtual environment, by applying force and torque feedback on a master device. Such devices are widely used in virtual reality,[1] gaming,[2] and tele-robotics.[3] In medicine, haptic devices are used for training in virtual environment for the practice of surgical techniques[4,5] or for tele-operation.[6–8] Currently, only few Minimally Invasive Surgery (MIS) robotic systems are available on the market. A well-known system is the da Vinci from Intuitive Surgical.[9] This system suffers from the lack of haptic feedback to the surgeon. Haptic feedback is rarely implemented in MIS robotic systems[9,10] and, at this time, no commercial system providing haptic feedback is available.[11–13] Several studies[14,15] reported that implementation of force feedback could widely reduce task completion time and error rate.

A previous study[16] highlights that MIS gesture requires at least four degrees of freedom (DoFs) to perform a suture (one translation and three rotations). Therefore, the haptic controller should have three rotations around the Remote Center of Motion (RCM) and one translation along its self-rotation axis. A tele-operated system has been developed to assist the surgeon during MIS procedures. This system is based on a master interface controlling a slave robot. The master device is called a haptic interface, which renders force feedback to the surgeon. The force feedback represents an additional benefit of the proposed system.[17]

* Corresponding author. E-mail: med.amine.laribi@univ-poitiers.fr

https://doi.org/10.1017/S0263574718000929 Published online by Cambridge University Press

This work is in line with the development of a teleoperation system for MIS.[16,19] A previous haptic interface based on parallel spherical architecture has been developed. This spherical parallel manipulator (SPM) suffers from the presence of the singularity inside the useful workspace. In this paper, a new architecture based on the use of a Delta structure is proposed. The challenging task is to obtain orientation DoFs from the Delta structure. The three translational DoFs are converted to two rotational DoFs. The third rotation as well as the translation along the self-rotation axis is provided by the added fourth leg. The proposed structure is similar to the one with 4 DoFs proposed by Clavel.[25] In our case, the fourth leg is made by universal joint, a prismatic joint and universal joint. This leg is used to transmit rotation from the base to the end-effector as well as to obtain the spherical motion. Most of haptic devices are developed on a Delta structure that is used to produce three translational DoFs. Delta structure has high kinematic performances, which will allow a well render of the force feedback. Parallel structures are known for high stiffness and accuracy.

Such a device based on Delta architecture has already been investigated by Suwelack *et al.*[18] to perform MIS simulation. A low-cost prototype has been developed using a Falcon haptic device. This prototype suffers from the lack of torque feedback along self-rotation axis and the lack of reliability.

This paper focuses on the kinematic model and the kinematic performances of the new interface based on Delta structure called 4haptic since it has four DoFs. The optimal solution of the new structure is obtained through dimensional synthesis problem formulated according to the workspace needed by MIS.

The paper is organized as follows. Section 2 presents the gesture analysis of MIS and an overview of a tele-operation system. The kinematic model of the new device is explained in Section 3. Section 4 compares the dexterity of the new interface to the one of the previous structure. Section 5 presents the formulation of the synthesis optimization problem used to obtain the optimal structure according to the predefined workspace. Section 6 concludes this paper by summarizing the main results obtained in the current work.

2. Gesture in Minimally Invasive Surgery and Tele-Operation

In this section, the expert's gesture analysis has been performed by a surgeon during MIS procedures. This analysis is based on the use of a motion-capture system. Using these results, the predefined workspace has been determined and a tele-operation system has been developed to assist the surgeon during several tasks.

2.1. Gesture analysis of minimally invasive surgery

Minimally Invasive Surgery uses instruments inserted into patient's body through tiny incisions points. Unlike open surgery which generally requires up to six DoFs, minimally invasive procedure requires only four DoFs: three rotations around the incision point and one translation along the instrument axis (as described in Fig. 1). This is due to the constraints imposed by the trocar.

An experimental analysis during an arterial anastomosis was made using a motion-capture system (Vicon). The system uses a set of high-resolution cameras to detect reflective markers placed on subjects that we want to study (see Figs. 2 and 3). Software (Nexus) allows to capture the scene, visualize, construct, and export the 3D position of each marker placed on the subject.

Multiple reflective markers have been placed on the instruments to evaluate their position and orientation (see Fig. 2). The expert has been performed arterial anastomosis on a pelvic trainer (see Fig. 3) in the same conditions as in an operating room. During these training, the software records the position of markers at frequency of 100Hz. Markers coordinates are then exported and processed under MATLAB.

The resulted data were used to evaluate the size of the tools workspace. The cone apex angle, α, is used to evaluate the workspace size generated by the axis of each tool. A cone is represented for each tool with a maximum value recorded on all manipulations performed in Cartesian space (see Fig. 4). One corresponds to the clamp with an angle of 17° and the second one is for the needle holder with an apex angle equal to 26°. Besides the rotations, each tool has also a translation motion along the axis of the cone represented by the maximum and minimum distance, respectively ($D_{\max}$) and ($D_{\min}$), between the point of incision and the tool tip. The self-rotation φ must be more than $\pm\ 180^\circ$.

https://doi.org/10.1017/S0263574718000929 Published online by Cambridge University Press

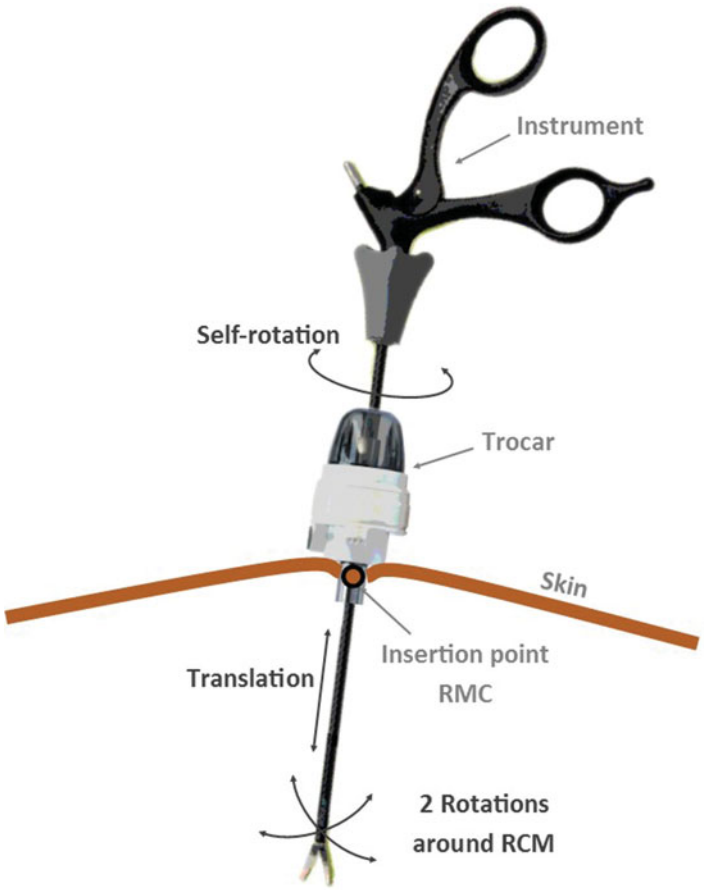


Fig. 1. Minimally invasive surgery motions.

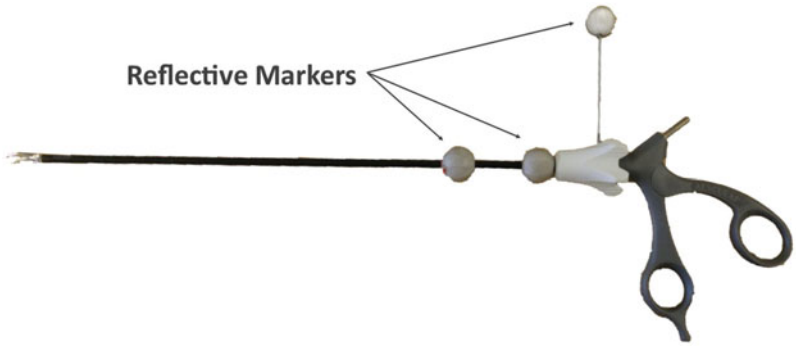


Fig. 2. MIS Instrument with reflective markers.

In the plan (ψ, θ), the workspace limit of the suture application is described by a pseudo-circular shape. Figure 5 shows the workspace limit and the captured orientations of the tool in the plan (ψ, θ). Through these results, it's clear that the more useful area of the workspace is at the center. Within this region, the developed haptic device should offer large kinematic performances as well as a uniform behavior. The evaluation criteria used in this work are based on kinematic performance of the manipulator (for more details see ref. [16]).

2.2. Tele-operated system for minimally invasive surgery

The main goal of tele-surgery is not to develop an autonomous system but to assist the surgeon during his task by adding accuracy and safety. Tele-operation systems are composed of a slave surgery robot controlled by a master interface (with or without haptic feedback).

https://doi.org/10.1017/S0263574718000929 Published online by Cambridge University Press

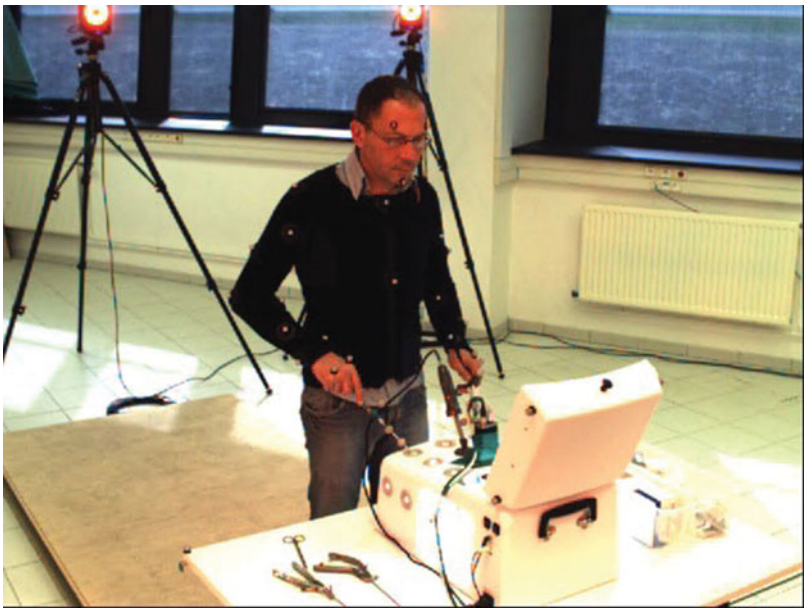


Fig. 3. Motion capture while performing an arterial anastomosis on a pelvic trainer.

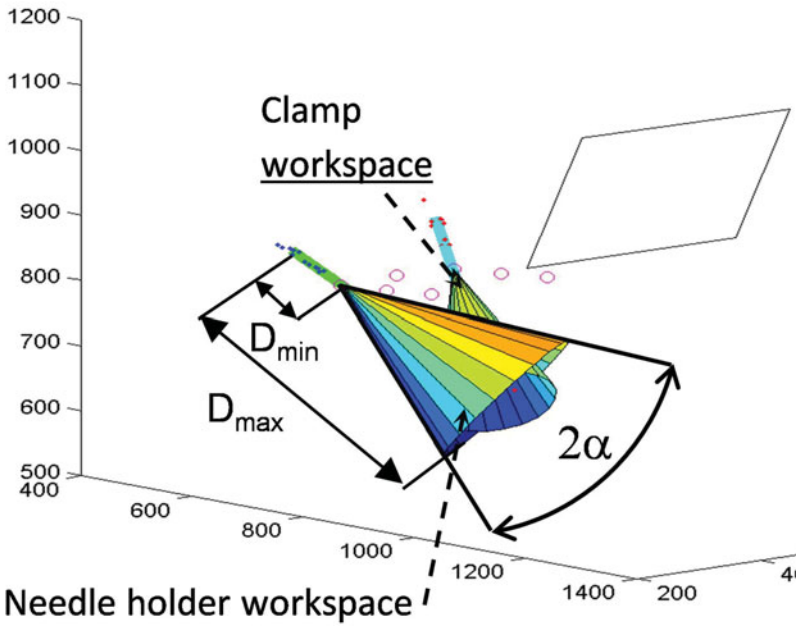


Fig. 4. A real tool needed workspace for MIS.

The slave station is composed of the two surgical robots and a camera as shown in Fig. 6. The slave robot was designed and optimized in order to perform MIS tasks based on the results of the gesture analysis. Each robot controls the motion of one instrument (a clamp and a needle holder). The camera is fixed and is pointed at the work area. The two robots are installed such that the tops of the instruments share the required workspace.

To describe the useful workspace, the slave robot was designed with a serial spherical architecture.

To implement haptic feedback on the master interface, a six-axis force sensor has been placed on the end of the slave robot, behind the effector.

https://doi.org/10.1017/S0263574718000929 Published online by Cambridge University Press

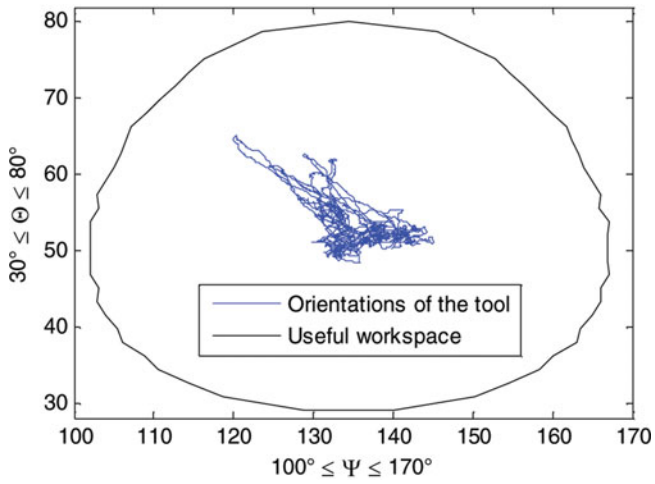


Fig. 5. Useful area of the workspace.

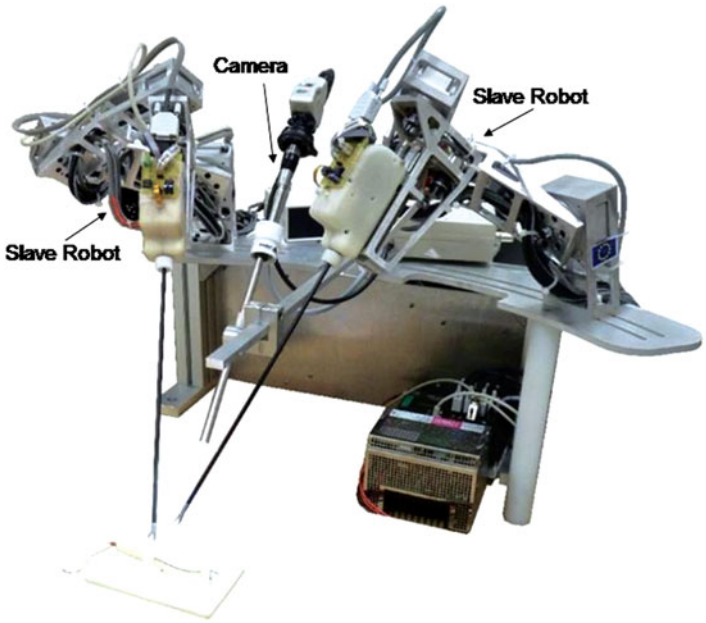


Fig. 6. MIS slave station.

A master interface (see Fig. 7) has been designed based on a spherical parallel architecture. Multiple prototypes of that interface have been developed. The first prototype suffers from the presence of a parallel singularity inside its workspace. This singularity is located in the center of useful workspace and depends on the self-rotation of the moving platform. It induces errors during Forward Kinematic Model (FKM) evaluation and requires high motor torques for haptic feedback.[19] Due to the singularity presence and poor kinematic performance, the first prototype does not allow us to properly control the slave robot.

To reduce effects of the singularity on haptic feedback, a redundant actuator was placed on the moving platform.[20] This setup allows us to obtain the needed torques for haptic feedback. However, it increases the weight of the moving platform. Accordingly, the haptic interface transparency is not improved anymore and makes it an improper solution to control the slave robot.

A novel kinematic based on Delta architecture is proposed in this work in order to develop a new haptic interface to cope with those drawbacks.

https://doi.org/10.1017/S0263574718000929 Published online by Cambridge University Press

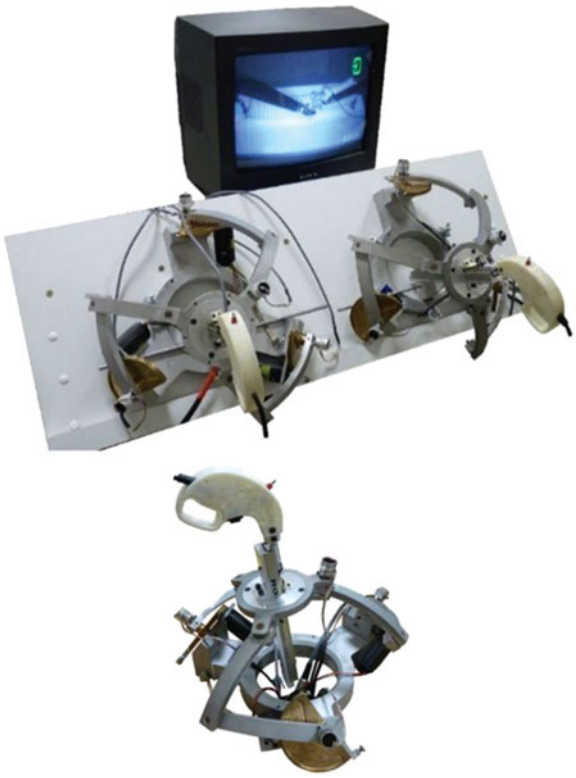


Fig. 7. MIS master station with spherical parallel architecture.

3. 4haptic Device Architecture

3.1. A novel kinematic

The novel kinematic of four DoFs haptic device is based on Delta architecture. However, classical Delta device allows three translational DoFs. To convert translations into rotations, a fourth leg is added to the structure. This extensible leg is linked with two spherical joints to the base and to the moving platform. The kinematics of the fourth leg is a prismatic followed by a universal joint. The three rotational DoFs, $\psi_e, \theta_e, \varphi_e$, are given by the orientation of that fourth leg relative to the base. The translational DoF, L_d, is given by the extension of that fourth leg (prismatic joint) as shown in Fig. 8.

The spherical joints on the center of the base and the moving platform are achieved with a universal joint each one. The composed spherical joint of the mobile platform is shown in Fig. 9. The self-rotation, φ_e, is supported by a revolute joint along the fourth leg, UPUR. The revolute joint, R, can be located before the universal joint (the case of Fig. 8) or after (on the ground). This solution allows a maximum angular rotation.

A 3D printed prototype was developed and presented in Fig. 10. This prototype was made to validate the new kinematic of the master device. The moving platform can be simply manipulated within the four DoFs.

3.2. Forward kinematic model

To evaluate the location of the moving platform, the coordinates of vector $\mathbf{OD} = [x_d, y_d, z_d]$ are expressed in the frame R_0, where O is the origin of the fixed frame attached to the base of the Delta and D is the center of the moving platform.

The geometric parameters of the new architecture are $L_1,\ L_2,\ r_a,\ r_d$ and α_i as described in Fig. 11. θ_1^i defines the active joint angle and $\theta_2^i,\ \theta_3^i$ the passive joint angles of each leg i, for $i = 1, 2, 3$. The coordinates of the center of the moving platform, point D, are given by the forward kinematic model

https://doi.org/10.1017/S0263574718000929 Published online by Cambridge University Press

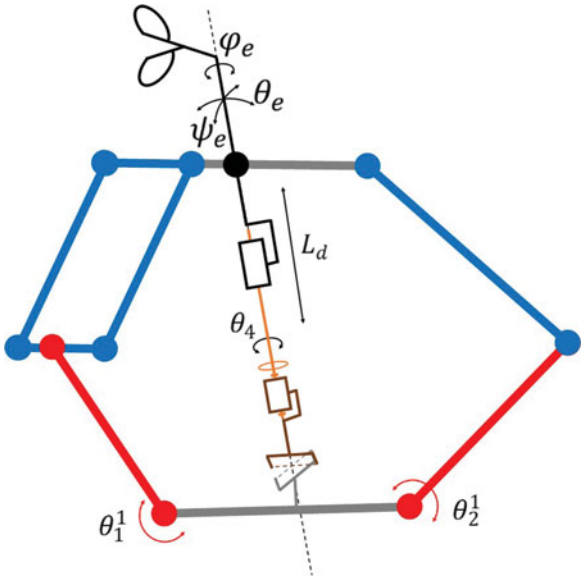


Fig. 8. New kinematic based on Delta robot architecture.

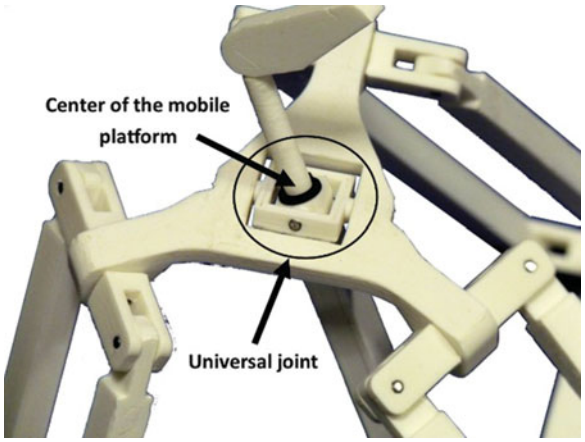


Fig. 9. Universal joint on the moving platform.

written as follows for each leg i of the Delta robot:

$$\begin{cases} x_D = C\alpha^i \left(r + L_1 C\theta_1^i + L_2 C\theta_3^i C\theta_{12}^i\right) - L_1 S\alpha^i S\theta_3^i, \\ y_D = S\alpha^i \left(r + L_1 C\theta_1^i + L_2 C\theta_3^i C\theta_{12}^i\right) + L_1 C\alpha^i S\theta_3^i \quad \text{for} \quad i = 1, 2, 3, \\ z_D = L_1 S\theta_1^i + L_2 C\theta_3^i S\theta_{12}^i, \end{cases} \tag{1}$$

with $r = r_a - r_d$ and $C\Theta = \cos(\Theta)$, $S\Theta = \sin(\Theta)$, $\Theta_{12} = \Theta_1 + \Theta_2$

The forward kinematic model computes the coordinates x_D, y_D, and z_D of the center of the moving platform for any given configuration of actuated revolute joints θ_1^i for $i \in \{1, 2, 3\}$. The position of point D can be obtained by solving the following equation:

$$(x_D - x_{Bi})^2 + (y_D - y_{Bi})^2 + (z_D - z_{Bi})^2 = L_2^2, \tag{2}$$

where

$$\begin{cases} x_{Bi} = \cos\left(\alpha^i\right)\left(r + L_1 \cos\left(\theta_1^i\right)\right) \\ y_{Bi} = \sin\left(\alpha^i\right)\left(r + L_1 \cos\left(\theta_1^i\right)\right) \\ z_{Bi} = L_1 \sin\left(\theta_1^i\right) \end{cases}. \tag{3}$$

https://doi.org/10.1017/S0263574718000929 Published online by Cambridge University Press



Fig. 10. 3D printed prototype of the 4haptic device.

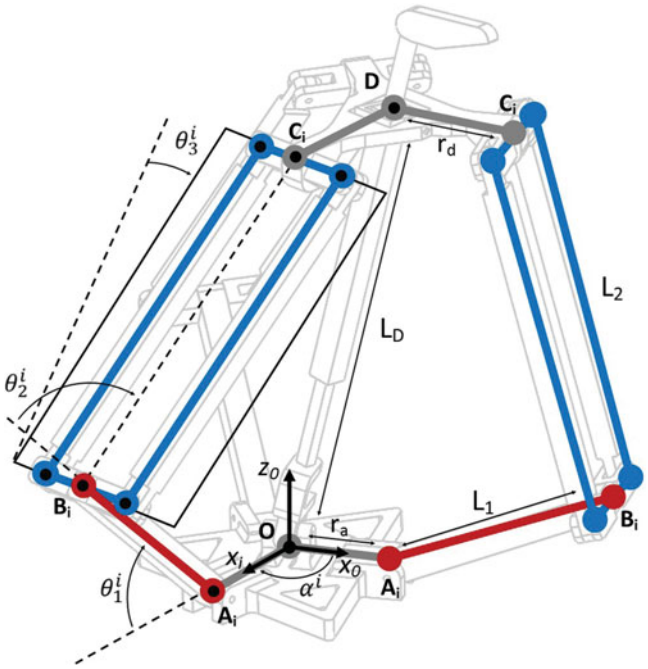


Fig. 11. Geometric parameters of the 4haptic device.

The orientation of the handle attached to the fourth leg is described using Euler *ZYZ* angles (ψ_e, θ_e, φ_e), as shown in Fig. 12. The self-rotation, φ_e, is directly given by the active joint θ_4 as shown in Fig. 8.

https://doi.org/10.1017/S0263574718000929 Published online by Cambridge University Press

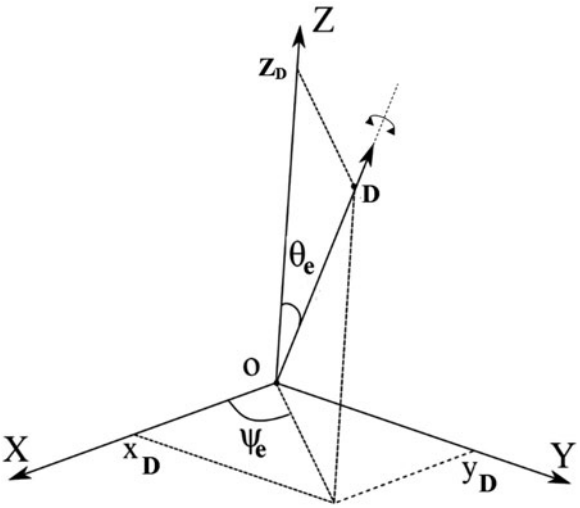


Fig. 12. Orientation of the 4th leg (vector **OD**).

Precession and nutation angles, ψ_e, θ_e, are computed using the coordinates of vector $\boldsymbol{OD}$ as follows:

$$\boldsymbol{OD} = L_{\mathrm{D}} \cdot \boldsymbol{R}_z(\psi_{\mathrm{e}}) \cdot \boldsymbol{R}_y(\theta_e) \cdot \boldsymbol{Z} = L_D \cdot \begin{bmatrix} \cos\psi_e \sin\theta_e \\ \sin\psi_e \sin\theta_e \\ \cos\theta_e \end{bmatrix} = \begin{bmatrix} x_D \\ y_D \\ z_D \end{bmatrix}, \tag{4}$$

with $L_D = ||\boldsymbol{OD}|| = \sqrt{x_D^2 + y_D^2 + z_D^2}$.

Finally, the expressions of the Euler angles are defined as follows:

$$\begin{cases} \theta_e = a\cos\left(\frac{z_D}{L_D}\right) \\ \psi_e = a\tan 2\left(\frac{y_D}{L_D \sin\theta_e}, \frac{x_D}{L_D \sin\theta_e}\right) \\ \varphi_e = \theta_4 \end{cases}. \tag{5}$$

The FKM model of the 4haptic device is solved for a given input vector $[\theta_1^1, \theta_1^2, \theta_1^3, \theta_4]^{\mathrm{T}}$ to evaluate $\theta_e, \psi_e, \varphi_e$, and L_D.

3.3. Inverse kinematic model

The inverse kinematic model (IKM) is solved for a given input vector $[\psi_e, \theta_e, \varphi_e, L_d]^{\mathrm{T}}$ to evaluate the actuated joint angles given by the output vector $[\theta_1^1, \theta_1^2, \theta_1^3, \theta_4]^{\mathrm{T}}$. The actuated joints are determined for a given position of the center of the moving platform, point D, using Eq. (6). This equation is obtained after substitution and rearrangement of Eqs. (2) and (5) for $i = 1, 2, 3$.

$$\begin{aligned} &2L_1 L_D \cos(\theta_e) \sin\left(\theta_1^i\right) + 2rL_1 \cos\left(\theta_1^i\right) - 2L_D \sin(\theta_e) \cos(\alpha - \psi_e)\left(r + \cos\left(\theta_1^i\right) L_1\right) \\ &\quad + L_D^2 + L_1^2 - L_2^2 + r^2 = 0. \end{aligned} \tag{6}$$

The previous equation can be rearranged in the following form:

$$l_i \cos\theta_1^i + m_i \sin\theta_1^i - n_i = 0, \tag{7}$$

where

$$\begin{cases} l_i = 2L_1\left(r - L_D \cos\left(\alpha^i - \psi_e\right) \sin(\theta_e)\right) \\ m_i = 2L_1 L_D \cos(\theta_e) \\ n_i = -2rL_D \cos\left(\alpha^i - \psi_e\right) \sin(\theta_e) L_D + L_1^2 - L_2^2 + L_d^2 + r^2 \end{cases}.$$

https://doi.org/10.1017/S0263574718000929 Published online by Cambridge University Press

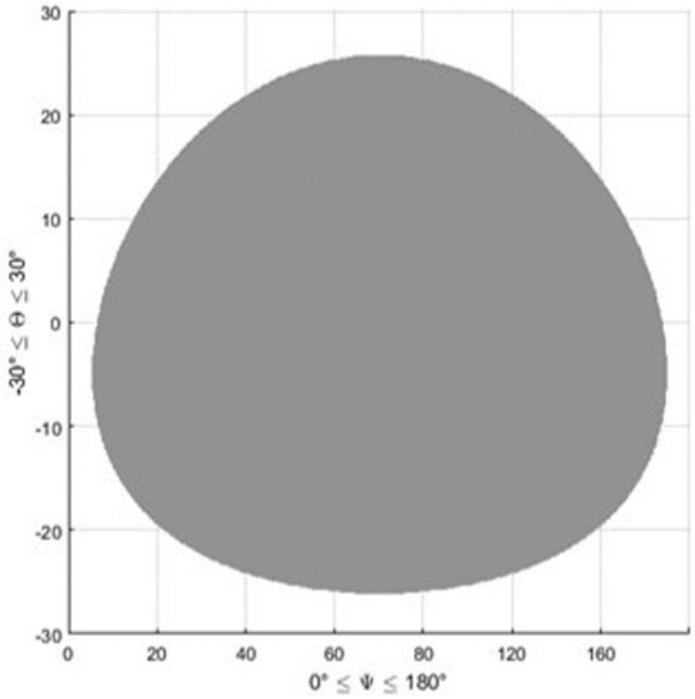


Fig. 13. Workspace in ψ, θ space for a given length $L_P = 100\,\text{mm}$.

Equation (7) has a solution if and only if

$$\left| \frac{n_i}{\sqrt{l_i^2 + m_i^2}} \right| \leq 1 \leftrightarrow n_i^2 - \left(l_i^2 + m_i^2\right) \leq 0. \tag{8}$$

More details on inverse kinematic model of Delta architecture can be found in ref. [21].

3.4. Workspace of the 4haptic device

The workspace of the 4haptic robot is defined by a region of the two-dimensional Euler space that can be attained by the handle along the fourth leg. The self-rotation φ_P of the handle is decoupled from the kinematic model and does not depend on the location of the mobile platform. The only constraints taken into account are the ones coming from the different chains given by Eq. (8), rewritten here as

$$g_i\left(\psi_P,\ \theta_P,\ L_P\right) = \left(2L_P \cos\left(\alpha^i - \psi_P\right) \sin\left(\theta_P\right)\left(-r + L_P \cos\left(\alpha^i - \psi_p\right) \sin\left(\theta_P\right)\right) + L_P^2 \cos\left(\theta_P\right)^2 + L_1^2 - L_2^2 + r^2\right)^2 - 4L_1^2\left(L_P^2 \cos\left(\theta_p\right)^2 + \left(r - L_P \cos\left(\alpha^i - \psi_P\right) \sin\left(\theta_P\right)\right)^2\right)^2 \leq 0. \tag{9}$$

where $g_i(\psi_P,\ \theta_P,\ L_P)$ represents a region attainable by the handle linked to the moving platform for a given branch. This equation represents a volume in Cartesian space. The boundary of this volume is defined by $g_i(\psi_P, \theta_P,\ L_P) = 0$ for $i = 1, 2, 3$.

To describe the whole workspace, the self-rotation φ_P is chosen as follows: $\varphi_P \in [-180^\circ; 180^\circ]$.

A given point P, with coordinates $(\psi_P,\ \theta_P,\ L_P)$, is inside the workspace of the 4haptic device only if $g_i(\psi_P,\ \theta_P,\ L_P) \leq 0$, $i = 1, 2, 3$, for every branch.

Figure 13 shows the workspace in Euler space for a given length L_P, here considered equal to 100 mm. More general representation of the workspace in ψ, θ, and L space is presented in Fig. 14. The same workspace can be built in Cartesian space as shown in Fig. 15, which describes an upper spherical cap.

https://doi.org/10.1017/S0263574718000929 Published online by Cambridge University Press

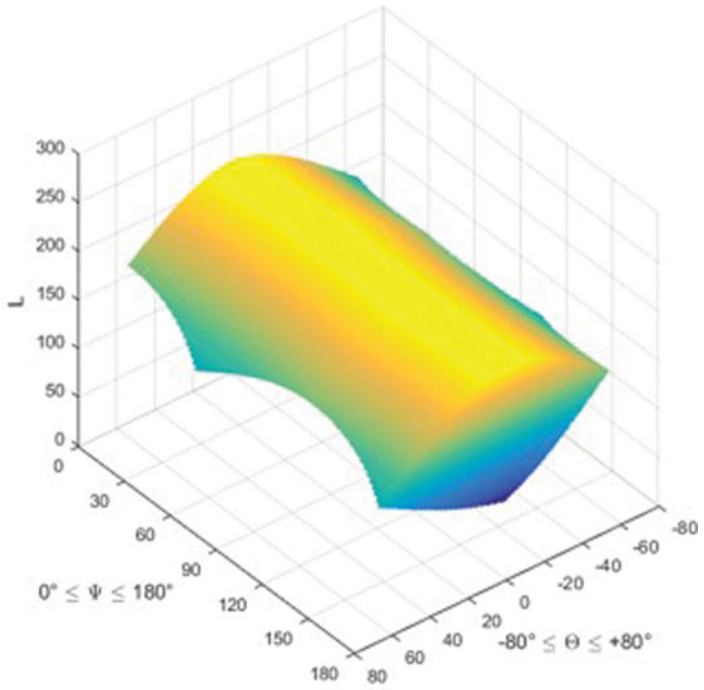


Fig. 14. Workspace in ψ, θ, and L space with $0^\circ < \psi < 180^\circ$, $-80^\circ < \theta < 80^\circ$, and 0 mm $< L <$ 250 mm.

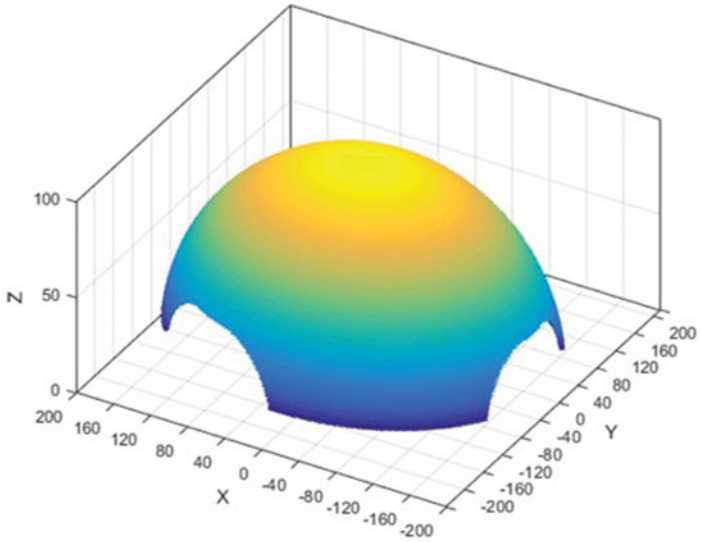


Fig. 15. Workspace in Cartesian space for a given length $L_P = 100$ mm.

4. Dexterity Analysis and Comparison Between SPM and the 4haptic Devices

The kinematic performances of a robot can be defined by the ability of a robot to perform motions around a point of its workspace. This ability is measured by the dexterity, which describes the amplification of the errors due to the kinematic and static transformations between Cartesian and joints spaces. Several methods exist in literature to compute this index.[19] The inverse of the condition number of Jacobian matrix $1/\kappa(\mathbf{J})$ is chosen in this work to evaluate the local dexterity that describes the kinematic for a given design vector $= [L_1, L_2,\ r,\ h]$.

https://doi.org/10.1017/S0263574718000929 Published online by Cambridge University Press

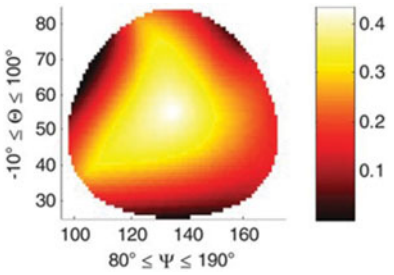


Fig. 16. Dexterity distribution for $\varphi = 0^\circ$.

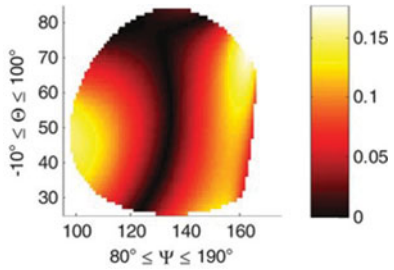


Fig. 17. Dexterity distribution for $\varphi = 50^\circ$.

The local dexterity is evaluated as follows:

$$\eta(\boldsymbol{J}) = \frac{1}{\kappa(\boldsymbol{J})}, \tag{10}$$

where $\kappa(\mathbf{J}) = \|\mathbf{J}\| \cdot \|\mathbf{J}^{-1}\|$.

4.1. SPM dexterity

The SPM dexterity has been evaluated in previous works.[19,20,22] The dexterity distribution on this architecture depends on the value of the self-rotation φ.

For MIS task, the center of the workspace is the most important region. According to the previous study of the SPM interface,[19] the dexterity reaches its maximum value on the center of the workspace, but it still low about 0.4. Figure 16 presents a dexterity distribution over the whole workspace for $\varphi = 0^\circ$. However, for $\varphi = 50^\circ$, the dexterity vanishes on the center of the workspace, as shown in Fig. 17. The presence of the singularity inside the workspace alters the kinematic performances and amplifies the error during FKM evaluation. The self-rotation is not controllable anymore when the mobile platform is close to the singularity regions. In addition, a high actuator torque will be requested for haptic feedback.

A solution with a redundant actuator installed on a joint of the platform has been studied.[20,22] This modification of the device improves the dexterity of the interface (up to 0.5). However, it increases the weight of the moving platform, which leads to an unsuitable solution.

4.2. 4Haptic dexterity

The Jacobian matrix of the 4haptic device, as a parallel robot, is composed of two matrices: parallel matrix $\mathbf{J_v}$ and serial matrix $\mathbf{J}_\theta$, see Eq. (11) as follows:

$$\boldsymbol{J_v v_D} = \boldsymbol{J_\theta \dot{q}}. \tag{11}$$

The Jacobian matrix in the input/output velocity relation is defined as follows:

$$\boldsymbol{v_D} = \boldsymbol{J\dot{q}}, \tag{12}$$

https://doi.org/10.1017/S0263574718000929 Published online by Cambridge University Press

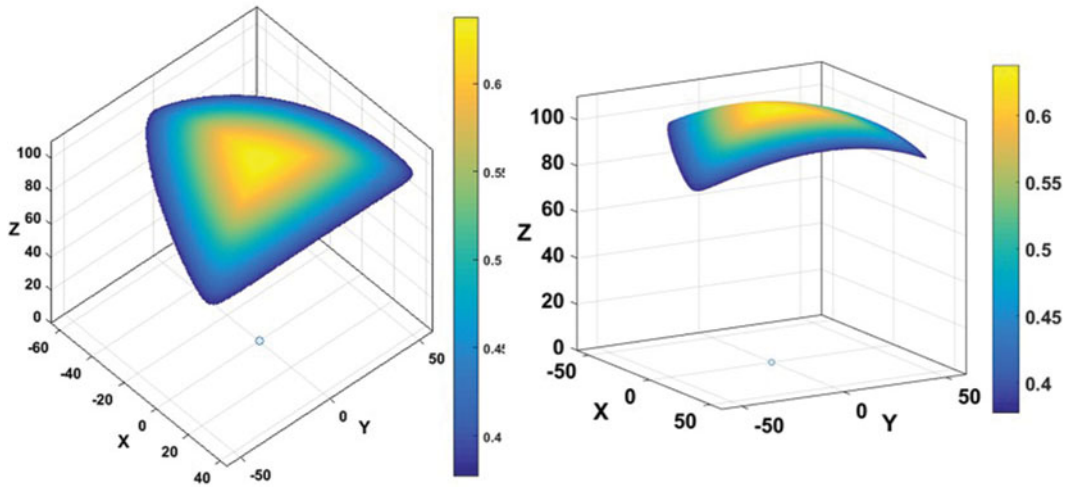


Fig. 18. Dexterity distribution of the 4haptic device in Cartesian space for $L_D =$ 100 mm.

with

$$\boldsymbol{J} = \left(\boldsymbol{J}_{\boldsymbol{v}}^{-1}\right)\boldsymbol{J}_{\boldsymbol{\theta}}. \tag{13}$$

$\mathbf{v_D} = [\dot{x}_D, \dot{y}_D, \dot{z}_D]^{\mathrm{T}}$ defines the platform velocity and $\dot{\mathbf{q}} = [\dot{\theta}_1^1, \dot{\theta}_1^2, \dot{\theta}_1^3]^{\mathrm{T}}$ defines joint velocities.

The matrices $\mathbf{J_v}$ and $\mathbf{J}_\theta$ can be obtained by differentiating the geometric equation (2). For the branch i (for $i = 1, 2, 3$), we can write

$$\begin{aligned} &\dot{x}_D\left(x_D - x_{Bi}\right) + \dot{y}_D\left(y_D - y_{B_i}\right) + \dot{z}_D\left(z_D - z_{Bi}\right) \\ &= \dot{x}_{Bi}\left(x_D - x_{Bi}\right) + \dot{y}_{Bi}\left(y_D - y_{B_i}\right) + \dot{z}_{Bi}\left(z_D - z_{Bi}\right). \end{aligned} \tag{14}$$

After substituting the differential expressions $\dot{x}_i$, $\dot{y}_i$, and $\dot{z}_i$ given by Eq. (15), the matrix form of Eq. (14) can be written and the Jacobian matrices are deduced:

$$\begin{cases} \dot{x}_{Bi} = -L_1 \cos\left(\alpha^i\right) \sin\left(\theta_1^i\right) \\ \dot{y}_{Bi} = -L_1 \sin\left(\alpha^i\right) \sin\left(\theta_1^i\right) \\ \dot{z}_{Bi} = L_1 \cos\left(\theta_1^i\right) \end{cases} \tag{15}$$

So, matrix $\mathbf{J_v}$ is a 3×3 matrix and is defined as follows:

$$\boldsymbol{J}_{\boldsymbol{v}} = \begin{bmatrix} x_d - x_{B1} & y_d - y_{B1} & z_d - z_{B1} \\ x_d - x_{B2} & y_d - y_{B2} & z_d - z_{B2} \\ x_d - x_{B3} & y_d - y_{B3} & z_d - z_{B3} \end{bmatrix}. \tag{16}$$

Matrix $\mathbf{J}_\theta$ is a diagonal 3×3 matrix and is defined as follows:

$$\boldsymbol{J}_{\boldsymbol{\theta}} = \boldsymbol{d}iag\begin{bmatrix} J_1 & J_2 & J_3 \end{bmatrix}, \tag{17}$$

with, for $i = 1, 2, 3$,

$$J_i = -L_1 C\alpha^i S\theta_1^i\left(x_D - x_{Bi}\right) - L_1 S\alpha^i S\theta_1^i\left(y_D - y_{B_i}\right) + L_1 c\theta_1^i\left(z_D - z_{Bi}\right). \tag{18}$$

Figures 17 and 18 depict the dexterity distribution of the 4haptic interface in Cartesian space and Euler space, respectively. Both distributions are computed for a fixed value of length L_D.

The new haptic interface presents a maximum local dexterity of 0.7. This value is greater than the one obtained for previous haptic device SPM,[19] which was limited to 0.4. In addition, no singularity region is to mention inside the 4haptic workspace.

https://doi.org/10.1017/S0263574718000929 Published online by Cambridge University Press

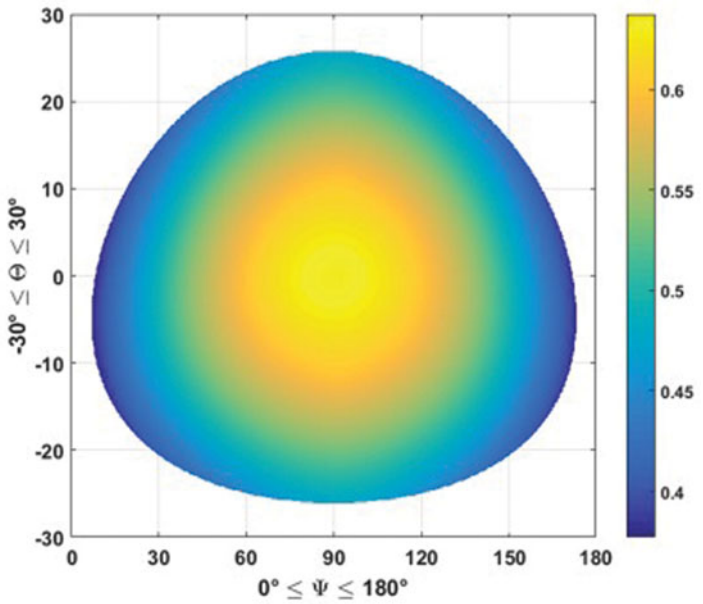


Fig. 19. Dexterity distribution of the 4haptic device in $\psi_e,\ \theta_e$ space for $L_D =$ 100 mm.

As shown in Fig. 19, the local dexterity reaches its maximum value at the center of the workspace and its distribution does not depend on the self-rotation φ_e. Since this rotation is decoupled for the case of 4haptic, all these make the new architecture more suitable and an adequate candidate for haptic interface for the surgical task.

5. Dimensional Synthesis of the 4haptic Device

5.1. Problem statement

This section deals with the formulation and the resolution of the nonlinear optimization problem of choosing the geometric design variables for the 4haptic device having a predefined workspace. This prescribed workspace has an associated volume W_s in space and described by a cone with an apex angle $\alpha = 26^\circ$ and a height of 112 mm. The predefined workspace corresponds to the one evaluated during gesture analysis (Section 2.1). Figures 21 and 22 present a spatial representation and a description of the predefined workspace considered in this work.

For every workspace to be swept by the 4haptic device, the independent design parameters are as follows:

$$\mathbf{I} = [L_1, L_2,\ r,\ h],$$

where

L_1 and L_2 : The lengths of the legs.

$r = r_a - r_d$: The difference of radius between the fixed platform and the moving one.

h : The position of the workspace on the $\boldsymbol{Z}$ axis defining how far is the specified volume from the fixed platform (see Fig. 20).

The objective of the optimization process is to find the set of parameters, given by $\mathbf{I_o} = [L_1^0, L_2^0, r^0, h^0]$, that can yield a 4haptic device having the smallest workspace containing a predefined region in space.

https://doi.org/10.1017/S0263574718000929 Published online by Cambridge University Press

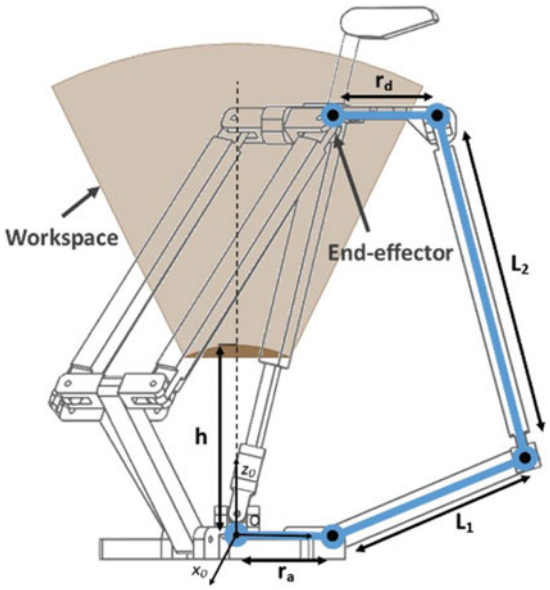


Fig. 20. Definition of optimized parameters.

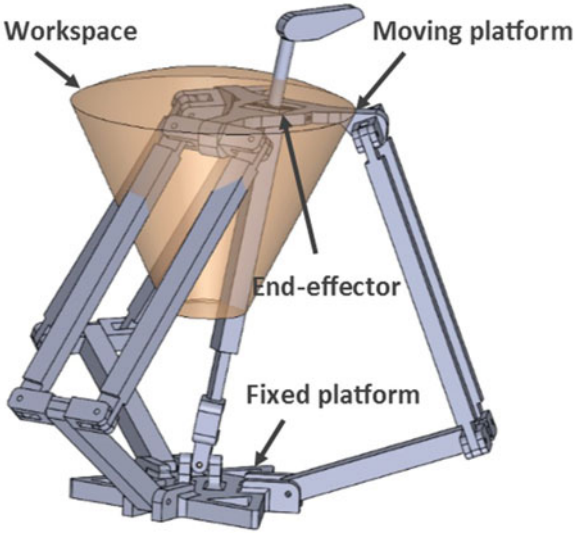


Fig. 21. Needed workspace and CAD model.

The adopted methodology here is to minimize an objective function that will depend on **I**. This minimization problem will be solved using the real-coded genetic algorithm (GA) method.[23,24]

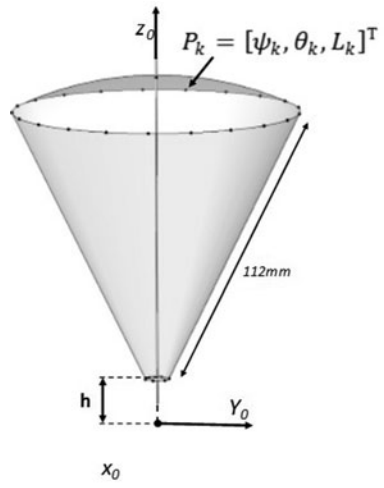
The optimization process can be summarized as follows:

$$\left|\begin{array}{l}\textbf{Input} \quad \text{Workspace definition (discretization on } \psi_p, L_p),\\ \textbf{Output} \quad \text{Optimal solution } \mathbf{I_o} = \left[L_1^0, L_2^0, r^0, h^0\right].\end{array}\right.$$

The optimization problem is constructed as follows:

$$\begin{array}{ll}\text{minimize} & F(\boldsymbol{I})\\ \text{subject to} & g_i(\mathbf{I},\ P) \le 0 \quad \text{for every points P inside the predefined workspace,}\end{array} \tag{19}$$

https://doi.org/10.1017/S0263574718000929 Published online by Cambridge University Press



	ψ_k [°]	θ_k [°]	L_k[mm]
Lower bound	0	0	h
Upper bound	360	26	$h + 112$

Fig. 22. The predefined workspace.

where $\mathbf{I} = [L_1, L_2,\ r,\ h]$ is the unknown design vector with the following allowable range for each parameter: $L_1,\ L_2\ \in [10\ ;\ 500]$, $r \in [0\ ;\ 100]$, and $h \in [10\ ;\ 300]$.

The objective function to minimize, $F(\mathbf{I})$, represents the sum of the powers of the vertices. This function uses the constraint functions $g_j(\mathbf{I},\ P)$ (defined by Eq. (9)), applied to the point P, which measure some kind of distance of this point with respect to the boundaries of the workspace. The boundaries of the workspace are defined by $g_j(\mathbf{I},\ P) = 0$. The boundaries of the workspace are also defined by the limits on the actuated joints. During this optimization process, actuated joints angles θ_i^1 have been bounded to$[-30^\circ\ ;\ 90^\circ[$, which avoid singular configurations of the Delta structure. To achieve this goal, the inverse kinematic model is applied to point P (using Eq. (7)) in order to evaluate actuated joint angles $\theta_1^1,\ \theta_2^1,$ and θ_3^1. If those angles are out of bound, a penalty is applied (see Eqs. (23) and (25)). The radius difference r between the mobile platform and the base is always considered positive ($r_d \leq r_a$).

A penalty function method is used to handle the constraints and to ensure that the fitness of any feasible solution is better than the infeasible ones.

The objective function is defined as follows:

$$F(\boldsymbol{I}) = F_1(\boldsymbol{I}) + F_2(\boldsymbol{I}) + F_3(\boldsymbol{I}), \tag{20}$$

where

$$F_1(\boldsymbol{I}) = \sum_{k=1}^{n} \sum_{i=1}^{3} \lambda_i(\boldsymbol{I}, P_k), \tag{21}$$

$$\begin{aligned} F_2(\boldsymbol{I}) &= \sum_{k=1}^{n} \sum_{i=1}^{3} |g_i(\boldsymbol{I}, P_k)| \\ F_2(\boldsymbol{I}) &= \sum_{k=1}^{n} \sum_{i=1}^{3} \Big| \Big[2L_P C\left(\alpha^i - \psi_P\right) S(\theta_P) \left(-r + L_P C\left(\alpha^i - \psi_p\right) S(\theta_P)\right) \\ &\quad + L_P^2 C(\theta_P)^2 + L_1^2 - L_2^2 + r^2 \Big]^2 - 4L_1^2 \left[L_P^2 C\left(\theta_p\right)^2 + \left(r - L_P C\left(\alpha^i - \psi_P\right) S(\theta_P)\right)^2 \right] \Big|^2, \end{aligned} \tag{22}$$

$$F_3(\boldsymbol{I}) = \sum_{k=1}^{n} \sum_{i=1}^{3} \mu_i(\boldsymbol{I}, P_k), \tag{23}$$

https://doi.org/10.1017/S0263574718000929 Published online by Cambridge University Press

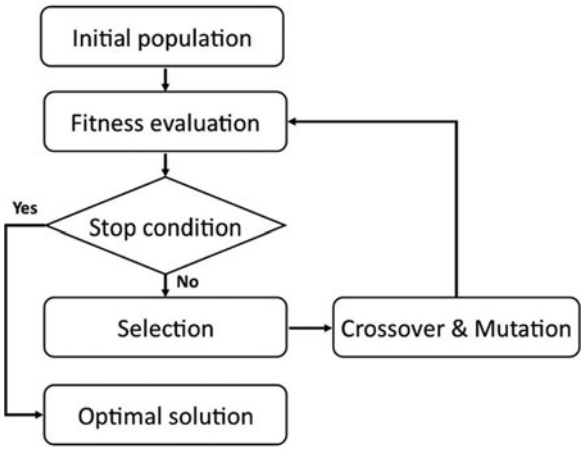


Fig. 23. Genetic algorithm flow chart.

where $P_k = [\psi_k,\ \theta_k,\ L_k]^{\mathrm{T}}, k = 1, .., K$, defines a point on the boundary of the predefined workspace (in this work, the predefined workspace is discretized in 721 points $P_k, k = 1, \ \ldots, \ 721$) and

$$\lambda_i\left(\boldsymbol{I}, P_k\right) = \begin{cases} 0 & \text{if } g_i\left(\boldsymbol{I}, P_k\right) \leq 0 \\ \chi_1 & \text{if } g_i\left(\boldsymbol{I}, P_k\right) > 0 \end{cases}, \tag{24}$$

$$\mu_i\left(\boldsymbol{I}, P_k\right) = \begin{cases} 0 & \text{if } \ -30^\circ \leq \theta_i^1\left(\boldsymbol{I}, P_k\right) < 90 \\ \chi_2 & \text{if } \ \theta_i^1\left(\boldsymbol{I}, P_k\right) < -30^\circ \ \textit{or} \ \theta_i^1\left(\boldsymbol{I}, P_k\right) \geq 90^\circ \end{cases}. \tag{25}$$

Here, χ_1 and χ_2 are large positive constants.

$F_1 \neq 0$ means that at least one point P_k is outside the 4haptic workspace. The function F_1 should be equal to zero to ensure that all the predefined workspace is within the robot workspace.

F_2 defines the power of a point P_k with respect to the boundary of the device workspace (which depends on the design vector). Therefore, minimizing $F_2(\mathbf{I})$ with respect to $\mathbf{I}$ is equivalent to finding the most compact structure that described the prescribed workspace W_S.

F_3 defines the actuated joints boundaries. Actuated joints have been limited to $[-30^\circ\ ;\ 90^\circ[$ in order to avoid singular configurations of Delta robot. $F_3 \neq 0$ means that at least one point P_k could not be reached by the parallel robot, taking into account joints limits. The function F_3 should be equal to zero to ensure that all point P_k could be reached by the Delta robot.

If $F_1(\mathbf{I}) > 0$, then the design vector $\mathbf{I}$ does not allow the structure to describe the predefined workspace W_S, and F_2 and F_3 are set to zero.

If $F_1(\mathbf{I}) = 0$, then $F_3(\boldsymbol{I})$ is evaluated.

If $F_3(\mathbf{I}) > 0$, then the design vector $\mathbf{I}$ does not allow the structure to reach all point P_k, taking joints limits into account. F_2 is set to zero.

If $F_3(\mathbf{I}) = 0$, then $F_2(\mathbf{I})$ is evaluated.

Figure 23 presents the flow chart of GA method applied to solve the optimization problem defined in Eq. (19). Initially the algorithm generates 300 sets of different design parameters as the first parent generation. Then, the three standard genetic operations, i.e., reproduction, crossover, and mutation, are performed to produce a new generation. Such procedures are repeated until the chosen number of generations is achieved, or the required accuracy leading to optimal solution $\mathbf{I}_0$ is satisfied. For every device generated, the workspace is calculated and compared to the predefined one. The latter operation is performed on 721 different points, P_k, on the workspace boundaries.

https://doi.org/10.1017/S0263574718000929 Published online by Cambridge University Press

Table I. The bounding interval for design variables.

I	L_1[mm]	L_2 [mm]	r [mm]	h [mm]
Lower bound	10	10	0	10
Upper bound	500	500	100	300

Table II. Optimal design parameters of the 4haptic device.

L_1	L_2	r	h
67 mm	76 mm	1 mm	10 mm

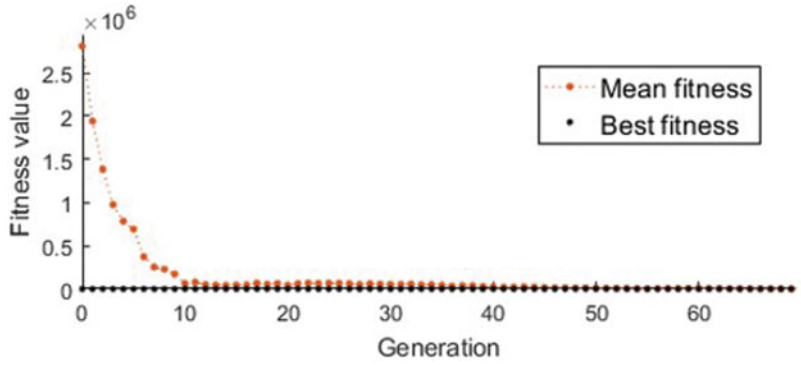


Fig. 24. Fitness function evaluation.

5.2. Results of optimization

This section presents the optimization results obtained using the GA method implemented under MATLAB. The bounding interval for each one of the design variables is presented in Table I.

The design parameters of the optimal solution of the 4haptic prescribing a needed workspace W_S, defined by a cone with a half apex angle of 26° and a translation of 112 mm, are given in Table II.

The GA has been running with a population of 300 individuals, with 200 generations per run. The optimal solution is found after 60 generations, as shown in Fig. 24.

Figures 25 and 26 represent horizontal slices of the workspace W_S at lower and upper boundaries in the Cartesian space. The gray area represents the space reachable by the 4haptic device (intersection of the workspaces of the three branches), whereas the orange one represents the needed workspace W_S, corresponding to the predefined one. Figures 25 and 26 show that the boundaries of W_S are located near the workspace boundaries of the 4haptic device.

Figure 27 shows the 3D CAD representation of the model of the 4haptic prototype device and the corresponding workspace along with the predefined volume. The 4haptic is build and designed using the optimal design parameters as defined in Table I. The volume in gray defines the workspace reachable by the 4haptic device. The volume in orange, defines the needed (predefined) workspace W_S. One can notice that all the points of the predefined workspace can be reached by the handle, which allows it to sweep the entire cone.

Figure 28 shows a slice at YZ plane of the workspace 3D model, which illustrates the optimal solution given in Table II obtained through the optimization process. This optimal solution yields the smallest workspace containing a cone located close to the boundary.

https://doi.org/10.1017/S0263574718000929 Published online by Cambridge University Press

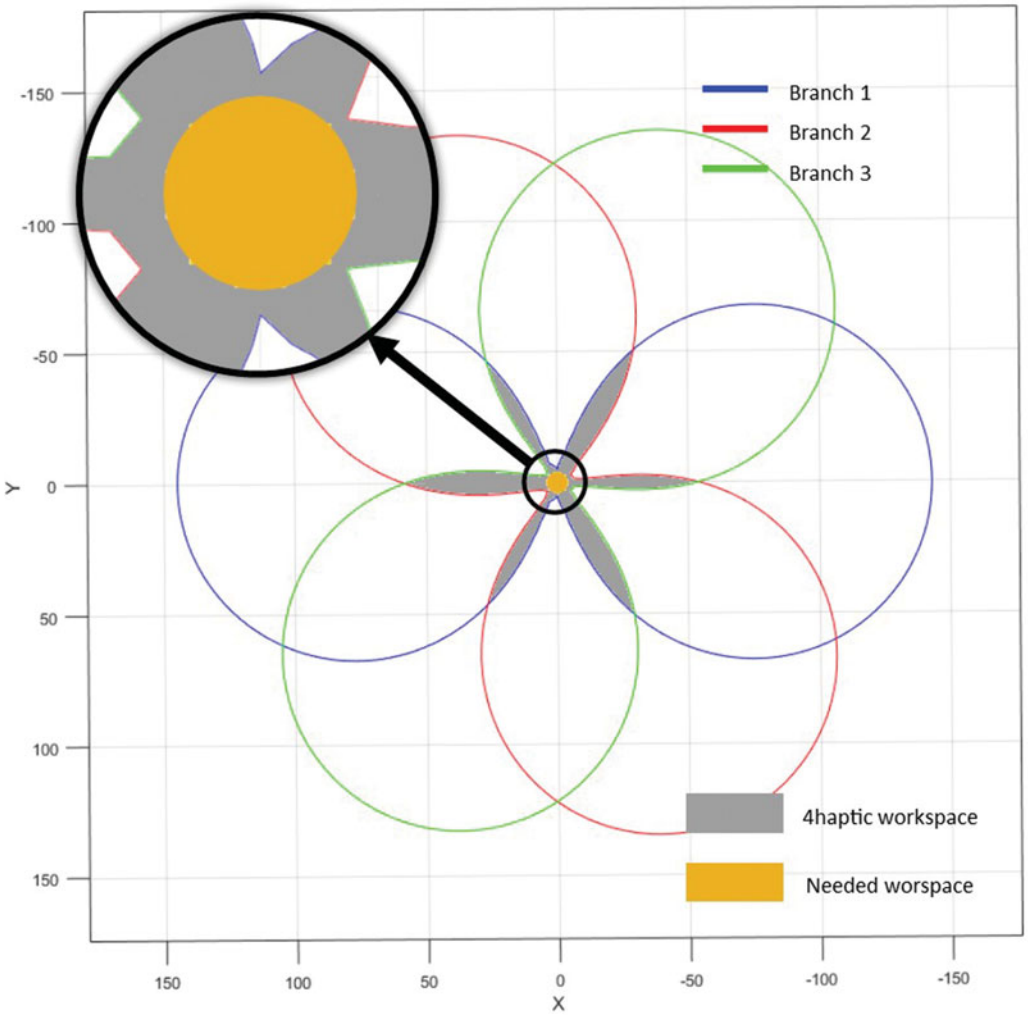


Fig. 25. Slice of the workspace for $z = 10$ mm.

6. Conclusion

This paper presents a novel kinematic architecture of a four DoFs haptic interface based on Delta structure called 4haptic. The challenging task was to obtain orientation DoFs from the Delta structure. A fourth leg is added to the Delta structure with the aim to convert translations into rotations and translation. This solution provides three rotations and one translation of the handle. The architecture as well as the kinematic model of the 4haptic device has been presented.

The dexterity distribution of the 4haptic device has been evaluated and compared with that of the existing haptic device based on the SPM architecture. The dexterity of the 4haptic device does not depend on self-rotation, which is an advantage comparing to the haptic SPM.

The comparison showed that the 4haptic presents an improved kinematic behavior and offers a singularity-free workspace. These advantages will improve the force feedback of the novel proposed device and make it a suitable haptic interface for MIS tele-operation systems.

An optimal dimensional synthesis method suited for the 4haptic device was presented in this paper. The design parameters of the optimal 4haptic, having the smallest workspace containing the predefined region in space identified by motion capture, have been obtained.

In future works, a multi-objective optimization problem will be introduced in order to maximize the dexterity as well as minimize the size of the structure. A prototype will be designed and built to control efficiently the surgical slave robot.

https://doi.org/10.1017/S0263574718000929 Published online by Cambridge University Press

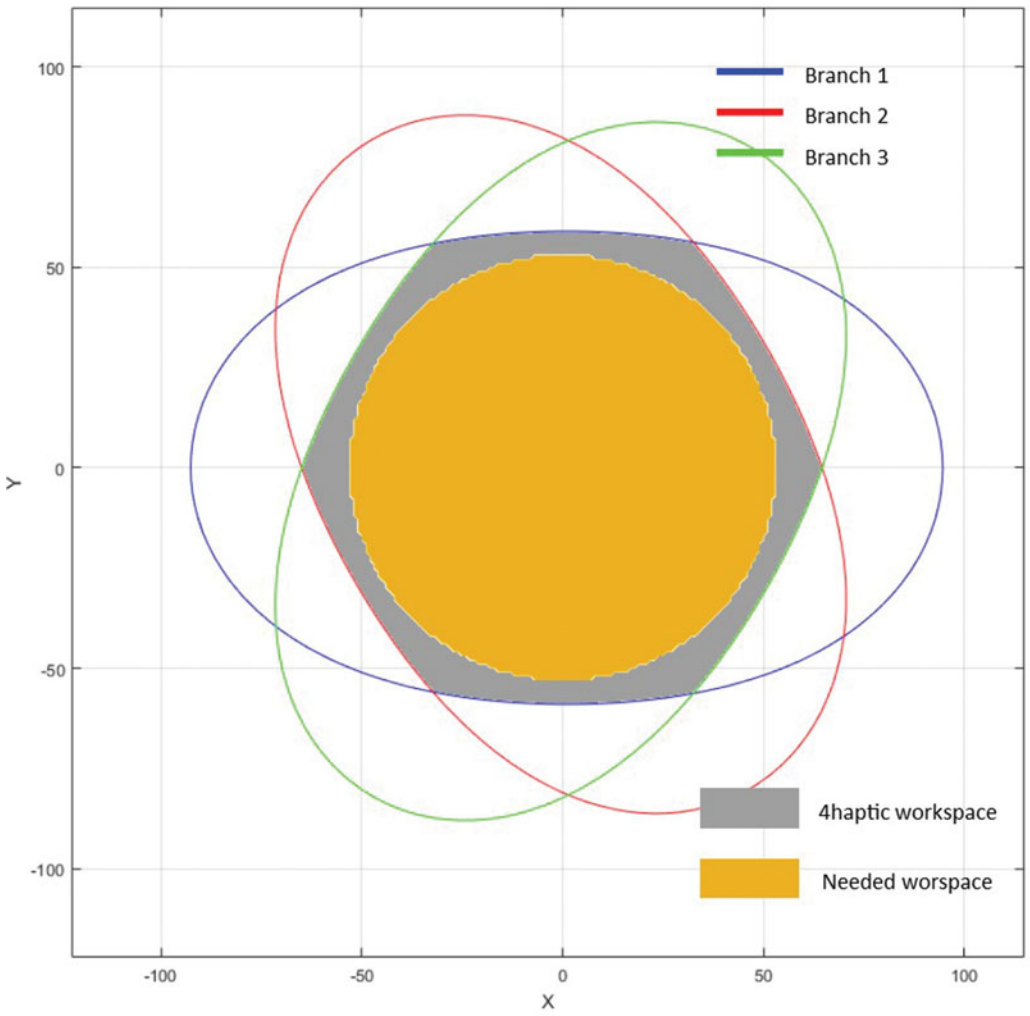


Fig. 26. Slice of the workspace for $z = 112$ mm.

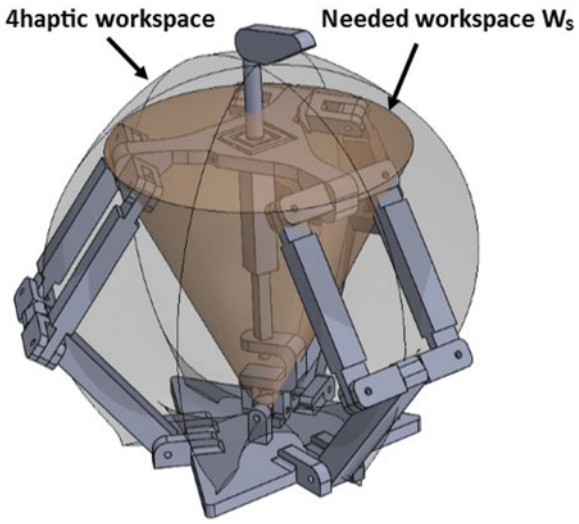


Fig. 27. The optimal 4haptic device.

https://doi.org/10.1017/S0263574718000929 Published online by Cambridge University Press

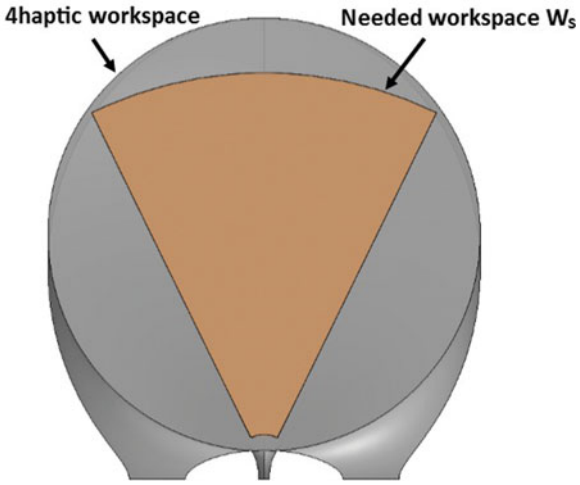


Fig. 28. Slice of the workspace in the *YZ* plane.

Acknowledgements
This research is supported by ROBOTEX, the French national network of robotics platforms (No. ANR-10-EQPX-44-01). This research is supported by the region Nouvelle-Aquitaine (program HABISAN 2015-2020) with the financial participation of the European Union (FEDER/ERDF, European Regional Development Fund).

References

1. F. Gosselin, T. Jouan, J. Brisset and C. Andriot, "Design of a Wearable Haptic Interface for Precise Finger Interactions in Large Virtual Environments," *Proceedings of the World Haptics 1st Joint Eurohaptics Conference and Symposium on Haptic Interfaces for Virtual Environment and Teleoperator Systems*, (2005) pp. 202–207.
2. W. Park, L. Kim, H. Cho and S. Park, "Design of Haptic Interface for Brickout Game," *Proceedings of the IEEE International Workshop on Haptic Audio visual Environments and Games*, (2009) pp. 64–68.
3. H. Son, A. Franchi, L. Chuang, J. Kim, H. Bulthoff and P. Giordano, "Human-centered design and evaluation of haptic cueing for teleoperation of multiple mobile robots," *IEEE Trans. Cybern.* **43**(2), 1247–1250 (2013).
4. J. Broeren, M. Rydmark and K. Sunnerhagen, "Virtual reality and haptics as a training device for movement rehabilitation after stroke: A single-case study," *Arch. Phys. Med. Rehabil.* **85**(8), 1247–1250 (2004).
5. Y.-W. Seo, A. Chowriappa, K. Guru and T. Kesavadas, "Medical Simulator for Trocar Insertion Procedure," Proceedings of the Medicine Meets Virtual Reality Conference, San Diego, CA (Feb. 2013).
6. L. van den Bedem, R. Hendrix, N. Rosielle, M. Steinbuch and H. Nijmeijer, "Design of a Minimally Invasive Surgical Teleoperated Master-Slave System with Haptic Feedback," *Proceedings of the International Conference on Mechatronics and Automation*, (2009) pp. 60–65.
7. A. Tobergte, P. Helmer, U. Hagn, P. Rouiller, S. Thielmann, S. Grange, A. Albu-Schaffer, F. Conti and G. Hirzinger, "The Sigma. 7 Haptic Interface for Microsurgery: A New Bi-Manual Surgical Console," *Proceedings of the IEEE/RSJ International Conference on Intelligent Robots and Systems* (2011) pp. 3023–3030.
8. L. Nouaille, M. A. Laribi, C. A. Nelson, T. Essomba, G. Poisson and S. Zeghloul, "Design process for robotic medical tool guidance manipulators," *Proc. Inst. Mech. Eng. Part C: J. Mech. Eng. Sc.* **230**(2), 259–275 (2016).
9. Intuitive Surgical, Inc., *The da Vinci Surgical System* (Intuitive Surgical, Inc.). Available at http://www.intuitivesurgical.com/products/davinci_surgical_system/
10. C. R. Wagner, Force Feedback in Surgery: Physical Constraints and Haptic Information *Ph.D. Thesis* (Cambridge: Harvard University, 2006).
11. H. G. Sim, S. K. Yip and C. W. Cheng, "Equipment and technology in surgical robotics," *World J. Urol.* **24**, 128–135 (2006).
12. V. Avgousti, E. G. Christoforou, A. S. Panayides, S. Voskarides, C. Novales, L. Nouaille, C. S. Pattichis and P. Vieyres, "Medical telerobotic systems: Current status and future trends," *Biomed. Eng. Online* **15**(96) (2016).
13. E. P. Westebring-van der Putten, R. H. M. Goossens, J. J. Jakimowicz and J. Dankelman, "Haptics in minimally invasive surgery-a review," *Minim. Invasive Therapy Allied Technol.* **17**(1), 3–16 (2008).
14. C. Wagner, N. Stylopoulos and R. Howe, "Force Feedback in Surgery: Analysis of Blunt Dissection," *Proceedings of the 10th Symposium on Haptic Interface for Virtual Environment and Teleoperator System*, Orlando (2002).

https://doi.org/10.1017/S0263574718000929 Published online by Cambridge University Press

15. C. E. Reiley, T. Akinbiyi, D. Burschka, D. C. Chang, A. M. Okamura and D. D. Yuh, "Effects of visual force feedback on robot-assisted surgical task performance," *J. Thorac. Cardiovasc. Surg.* **135**, 196–202 (2008).
16. A. Chaker, A. Mlika, M. A. Laribi, L. Romdhane and S. Zeghloul, "Synthesis of spherical parallel manipulator for dexterous medical task," *Front. Mech. Eng.* **7**(2), 150–162 (2012).
17. O. A. J. van der Meijden and M. P. Schijven, "The value of haptic feedback in conventional and robot-assisted minimal invasive surgery and virtual reality training: A current review," *Surg. Endosc.* **23**(6), 1180–1190 (2009).
18. S. Suwelack, C. Sander, J. Schill, M. Serf, M. Danz, T. Asfour, W. Burger, R. Dillmann and S. Speidel, "Towards open-source, low-cost haptics for surgery simulation," *Stud. Health Technol. Informat.* **196**, 401–403 (2014).
19. H. Saafi, M. A. Laribi and S. Zeghloul, "Forward kinematic model improvement of a spherical parallel manipulator using an extra sensor," *Mech. Mach. Theory* **91**, 102–119 (2015).
20. H. Saafi, M. A. Laribi and S. Zeghloul, "Redundantly actuated 3-rrr spherical parallel manipulator used as a haptic device: Improving dexterity and eliminating singularity," *Robotica* **33**(5), 1113–1130 (2015).
21. F. Pierrot, C. Reynau and A. Fourier, "DELTA: A simple and efficient parallel robot," *Robotica* **8**, 105–109 (1990).
22. H. Saafi, M. A. Laribi and S. Zeghloul, "Optimal torque distribution for a redundant 3-RRR spherical parallel manipulator used as a haptic medical device," *Robot. Auton. Syst.* **89**, 40–50 (2017).
23. M. A. Laribi, L. Romdhane and S. Zeghloul, "Analysis and dimensional synthesis of the delta robot for a prescribed workspace," *Mech. Mach. Theory* **42**(7), 859–870 (2007).
24. The MathWorks Inc., MATLAB and Optimization Toolbox, Release 2016b. The MathWorks Inc., Natick, Massachusetts, USA (2016).
25. R. Clavel, Device for the movement and positioning of an element in space, US Patent 4,976,582 (1990).

https://doi.org/10.1017/S0263574718000929 Published online by Cambridge University Press